Investigations of Feldspar-Quartz Raw Materials After Firing: Effect of Various Na$_2$O/K$_2$O Ratio and Synthetic Pigments Addition

Ewa Lewicka [1],* and **Anita Trenczek-Zajac** [2]

[1] Mineral and Energy Economy Research Institute of the Polish Academy of Sciences, J. Wybickiego 7A, 31-261 Kraków, Poland

[2] Faculty of Materials Science and Ceramics, AGH University of Science and Technology, al. A. Mickiewicza 30, 30-059 Kraków, Poland; anita.trenczek-zajac@agh.edu.pl

* Correspondence: lewicka@min-pan.krakow.pl

check for updates

Abstract: Different techniques (chemical analysis, X-ray diffraction, Mössbauer spectroscopy, UV-Vis-NIR spectrophotometry and chromaticity measurements) were used to study the color variation of feldspathic raw materials after firing at 1200 °C. Two varieties of feldspar-quartz grits (with Na$_2$O or K$_2$O prevalence) doped with synthetic pigments (hematite and rutile) were heat-treated in an oxidizing atmosphere. The results obtained indicate that the color of the ceramic body after firing may not only depend on the presence and analytical content of coloring elements (such as iron and titanium), but on their valence state and the chemical characteristics of the melt itself. The prevalence of larger alkali K$^+$ ions over Na$^+$ ions may cause the reduction of the coordination number of iron. This has a significant effect on the length of the Fe–O bond, which in turn influences the capacity for light absorption of a specific wavelength. The results of spectrophotometric measurements showed pronounced disparity between the raw materials and samples doped with coloring oxides. The introduction of synthetic pigments caused clear changes in the spectral dependence of the total absorbance. The absorbance increased in the whole measuring range, in particular in the visible part of the spectrum. Furthermore, a red-shift of the absorption bands towards longer wavelengths attributed to oxygen-metal charge transfer (OMCT) interactions between Fe^{3+} and O^{2-} ions as well as to d-d transitions within Fe^{3+} ions was observed.

Keywords: potassium- and sodium-rich feldspar-quartz; coloring oxides; Mössbauer spectroscopy; UV-Vis-NIR spectrophotometry; color after firing

1. Introduction

Feldspars are the most common raw materials used as fluxes in the ceramics industry. Compared to other components of the ceramic body (e.g., ceramic clays and quartz), the low melting point of feldspars means that they form a vitreous phase contributing to the sintering of a given mixture of constituents in the course of firing. In Poland, the basic source of feldspathic raw materials (feldspar-quartz) are deposits located in Lower Silesia (SW Poland), in the marginal zone of the Strzegom-Sobótka leucogranite massif. These rocks developed as a result of metasomatic alteration of various types of granite in the contact zone of magma intrusion with surrounding rocks (gabbro, serpentinite and amphibolite) of the Carboniferous age [1]. Metasomatic transformation of the rocks was followed by enrichment of their mineral composition in feldspar minerals (plagioclases and microcline-type perthite).

The major domestic manufacturer of feldspar-quartz commodities is the Strzeblowskie Mineral Mines (SKSM) of Sobótka, operating four deposits of granitoids located in the NW part of the outer

zone of the massif. The excavated raw material is characterized by considerable mineral and chemical differentiation and quite a high content of coloring oxides (0.2–0.7% Fe_2O_3 + TiO_2 [2]). To obtain stable and repeatable parameters of commercial product with fixed chemical composition tailored to customer requirements, the raw material is selectively extracted from each deposit. Afterwards, it is examined for chemical composition at consecutive stages of processing (crushing, sieving, and blending). Another crucial parameter that needs to be controlled is the color after firing, as the main customer of these commodities is the domestic ceramic tile industry [3].

The aim of the present study was to assess the influence of chemical composition of the raw material (especially alkalis and coloring oxides) on the color of the sintered body. In addition, this study sought to identify mineral phases that occur as a result of heat treatment of two commercial grades of feldspar-quartz grits from SKSM, with special attention to iron- and titanium-bearing ones, as they are the most common chromophores. The research was also focused on interaction between iron and titanium ions in the course of firing. Appropriate control of the chemical composition of the raw materials used in the ceramics industry has fundamental significance for properties and aesthetic qualities of the final products.

2. Materials and Methods

The raw material from deposits located in the Sobótka region consists of well-characterized mineral components [4,5]. According to previous studies, the main minerals containing coloring elements are: chlorites, micas (biotite, muscovite and sericite), rutile, garnets, feldspars, monazite, zircon, xenotime, epidote (Fe-rich pistacite), magnetite, pyrite and Fe-Ti spinel (titanomagnetite). The basic constituent of the raw materials after firing is the amorphous phase, resulting from thermal decomposition of feldspars and partly quartz, accompanied by single quartz grains and other minerals characterized by high melting temperatures, such as zircon, Fe-Ti spinel, xenotime and monazite [5,6].

The subject of the current research was feldspar-quartz commodities provided by the Strzeblowskie Mineral Mines of Sobótka. The samples represented two commercial grades of feldspathic grits of different moduli $K_2O:Na_2O$, i.e., with the prevalence of potassium or sodium particles in the chemical composition ($K_2O:Na_2O$ = 1.8 or 0.6, respectively, Table 2).

From each type of the raw material there were four samples prepared: the starting/basic ones (marked 0, Figure 1), and three others doped with controlled quantities of Fe_2O_3—hematite—and TiO_2—rutile (designated as I, II and III), as indicated in Table 1. Thorough homogenization of the basic material with coloring oxides was obtained by dry milling in a planetary ball mill for around 40 min. The pigments used in the experiment were synthetic ferric red TP-303 (Nofar) of 99.2% Fe_2O_3 purity and titanium white Tytanpol ®R-001 of 99.1% TiO_2 purity.

Table 1. The percentages of synthetic pigments added to basic samples of feldspar-quartz raw materials (wt. %).

Sample	Fe_2O_3	TiO_2
I	1.5	-
II	-	0.5
III	1.5	0.5

The chemical compositions of the studied materials were quantified by the wavelength dispersive X-ray fluorescence method (WDXRF) on a Bruker AXS (Karlsruhe, Germany) S8 TIGER spectrometer with a 3 kW Rh anode X-ray tube. The spectrometer is equipped with a Bruker's Quant-Express software allowing for standardless analysis of elemental composition of the samples. Quant-Express comprises a customized calibration prepared by Bruker using the feldspar-quartz rock of interest and selected certified reference materials. The accuracy of the measurements was determined by the instrument supplier (Table 2). After grinding (d90 = 53.3 µm) and mixing with a few drops of distilled

water, the 20 g portions of the material were pressed into pellets of ca. 40.4 mm diameter and maximum 10 mm thickness in a stainless-steel matrix of a Herzog TP 20 P hydraulic press with a pressure of 100 kN. The pellets were fired for 51 min in an oxidizing atmosphere in an electric furnace (Nabertherm LS 25/13). The maximum temperature 1200 °C was reached in 22 min (starting from room temperature) with a ramp rate of 54.5 °C/min. After 6 min holding time at 1200 °C the samples were quickly cooled down to 95 °C at a rate of 48.04 °C/min (for 23 min) in a furnace with integrated fans, then removed to air-cool to room temperature. These conditions (temperature and time) are usually adopted in the current fast-firing technology of ceramic tile production. After cooling, the samples were examined by X-ray diffraction, Mössbauer spectroscopy, UV-Vis-NIR spectrophotometry and chromaticity analysis.

Figure 1. Color after firing of the studied samples: potassium (K) and sodium (Na) types doped with synthetic pigments (marked I-III) plus that of the basic samples (marked 0).

Table 2. Analyzed weight % composition of the studied feldspar-quartz raw materials.

Sample	SiO_2	Al_2O_3	Fe_2O_3	TiO_2	Na_2O	K_2O	CaO	MgO	LoI
Max. deviation	±2.0	±0.150	±0.010	±0.005	±1.0	±0.30	±0.30	±0.05	n.d.
Potassium-rich samples									
0 K	75.90	13.93	0.30	0.053	2.87	5.14	0.20	0.16	1.19
I K	73.18	14.46	1.77	0.055	2.96	5.23	0.22	0.16	1.62
II K	73.56	14.79	0.34	0.566	3.05	5.33	0.22	0.17	1.59
III K	72.46	14.51	1.85	0.545	3.00	5.27	0.21	0.16	1.69
Sodium-rich samples									
0 Na	73.78	15.20	0.36	0.096	5.48	3.49	0.38	0.13	0.98
I Na	71.90	15.23	1.77	0.042	5.38	3.56	0.38	0.14	1.24
II Na	72.57	15.40	0.29	0.537	5.48	3.58	0.38	0.13	1.23
III Na	71.80	14.97	1.75	0.536	5.31	3.50	0.38	0.13	1.27

n.d.—not determined.

The mineral phases were identified by X-ray powder diffraction (XRD). The data were collected by a Rigaku MiniFlex 600 X-ray diffractometer (Neu-Isenburg, Tokyo, Japan) with the curved crystal graphite-monochromatized CuKα radiation, operating with a voltage of 40 kV and an emission current of 15 mA. XRD patterns were recorded in the angular range 3–75° 2Θ with a step size of 0.05°, counting time

1 s per step. The examinations were performed for feldspar-quartz samples of both types, before and after firing.

The Mössbauer spectra were collected using the RENON MsAa-3 spectrometer equipped with LND detector with Kr filter and laser interferometer He-Ne at room temperature [7]. A commercial ^{57}Co (RH) isotope was used as a source of radiation. All spectra shifts were reported versus the total shift in α-Fe. The obtained spectra were processed by the MOSGRAF-2009 software. There were four samples analyzed: two samples of sodium feldspar-quartz doped with one and two coloring oxides (I Na and III Na) and two corresponding samples of potassium feldspar-quartz (I K and III K).

The optical properties of selected samples after firing were analyzed based on the spectral dependence of the absorbance (A). The spectra were recorded in a broad wavelength range (λ) of 220 to 2200 nm with a Jasco V-670 UV-VIS-NIR double-beam spectrophotometer equipped with a dedicated 150-mm integrating sphere to perform the measurements of the total absorbance. The measured parameter was the reflectance (scale 0–100%), which was converted into the absorbance and analyzed. Such a calculation was feasible because the samples thickness was incomparably greater than the wavelength of the light used (10 mm vs. 220–2200 nm). The integrating sphere was coated with barium sulfate and the spectra were referenced against white standard—Spectralon. The applied speed was 200 nm/min with a step of 0.5 nm.

A portable Konica Minolta CM-2300d spectrophotometer was used to determine the chromatic coordinates of fired samples. The Konica Minolta CM-2300d instrument of spherical type with horizontal alignment, is suitable for complex color analysis in the visible wavelength range (400–700 nm). Color coordinates L*, a* and b* values of the specimens were obtained in CIE 1976 (Commission Internationale de l'Éclairage) space, where L* refers to darkness-brightness (0–100), a* to the red (a* > 0) or green (a* < 0), and b* to yellow (b* > 0) or blue (b* < 0).

3. Results

3.1. Chemical Composition

Table 2 lists the chemical composition of the studied samples. The difference in K_2O, Na_2O and Al_2O_3 content between samples of sodium and potassium influences the amount of amorphous phase during firing. Furthermore, the basic potassium sample (0 K) contains slightly less Fe_2O_3 and TiO_2, which are the main color contributors, as compared to its sodium counterpart (0 Na).

3.2. The XRD Analyses

The X-ray diffraction analyses of the studied samples only provided information on the main mineral phases because many of the peaks corresponding to minor phases coincided with major ones. The predominant crystalline phases of the raw (unfired) sample of sodium feldspar-quartz (marked Na raw) were: albite (d—4.02, 3.78, 3.67, 3.19 and 2.93 Å) and β-quartz (d—4.29, 3.35, 1.82 and 1.54 Å), as well as—albeit less numerous—microcline (d—4.26, 3.84, 3.48, 3.28 and 3.24 Å) (Figure 2). In addition, some faint reflections of illite (d—10.0, 4.46, 3.36 and 2.86 Å) and kaolinite (d—7.05, 4.48, 3.58, 3.85 and 2.55 Å) were also registered. The diffraction pattern of the sample after firing (0 Na) evidenced the presence of a characteristic amorphous hump within the 2Θ 15–40° range associated with the existence of the glassy phase, as well as remnants of quartz and albite that were not completely melted. Some small peaks indicating the secondary mullite (probably) precipitation were also registered (d—5.37, 3.43, 3.37 and 1.46 Å). Sodium-rich variety samples doped with synthetic pigments (I Na and III Na) gave weak hematite peaks (d—2.69, 2.51, 1.68 and 1.46 Å) and a much larger hump of an amorphous phase, which arose mainly at the expense of albite. The thermal decomposition of albite may be attributed to a high iron oxide content. It is well known that in silicate melts iron may occur in both oxidation states, as Fe^{2+} and Fe^{3+} ions [8,9], of which Fe^{2+} acts as a network modifier (flux) and thereby lowers the melting point and viscosity [10,11].
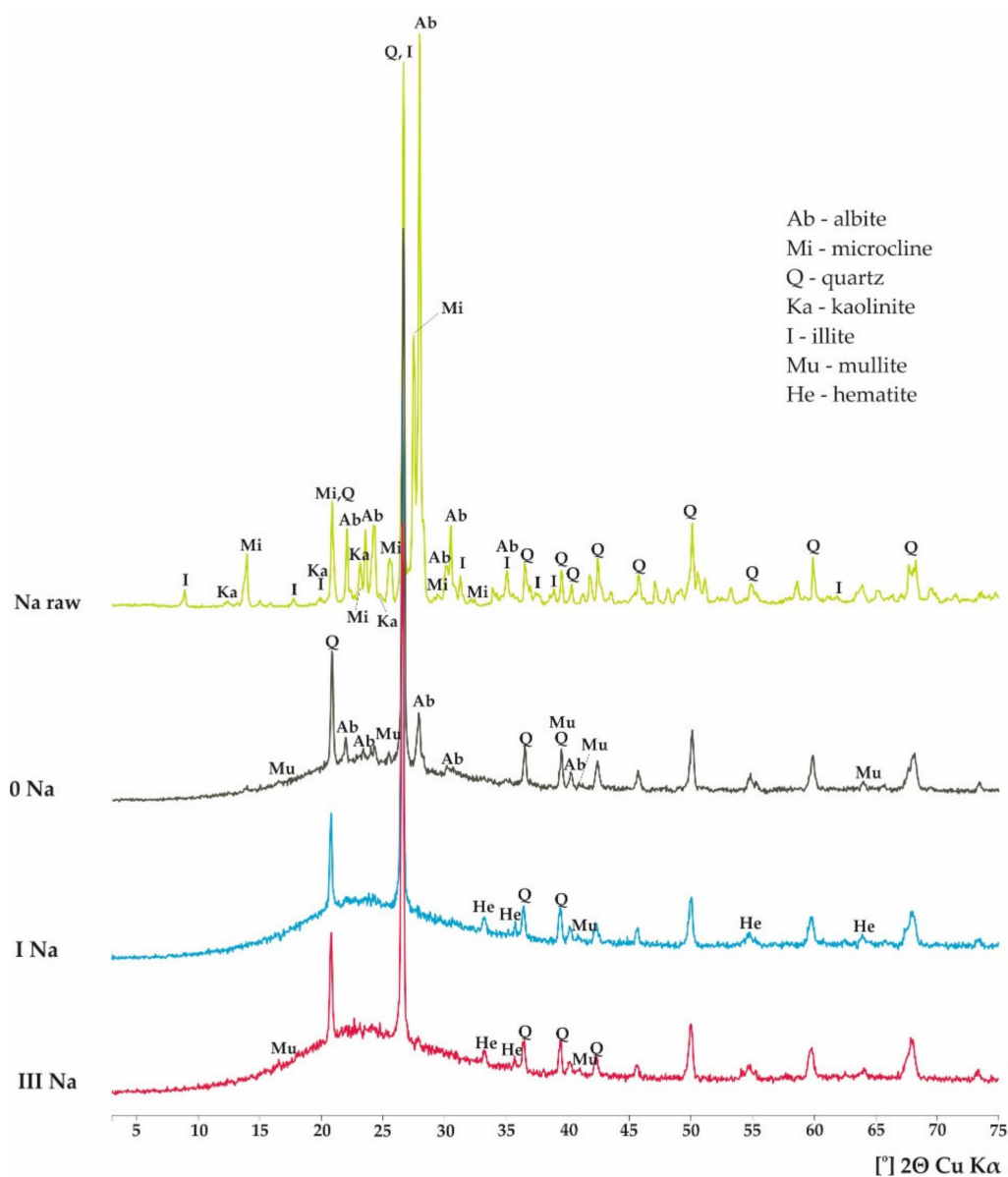
Figure 2. XRD patterns of sodium feldspar-quartz samples in a raw state/unfired (Na raw), as well as the samples after firing: without synthetic pigments addition (0 Na), as well as doped with 1.5% Fe_2O_3 (I Na), and with 1.5% Fe_2O_3 + 0.5% TiO_2 (III Na).

According to the XRD analysis of the unfired sample of the potassium variety raw material (K raw) its main mineral phases are: β-quartz (d—4.26, 3.34, 2.46, 1.82 and 1.54 Å) and microcline (d—4.20, 3.83, 3.30, 3.24, 3.02 and 2.96 Å) (Figure 3). Some smaller reflections of albite (d—4.03, 3.83, 3.77, 3.66, 3.19, 2.95 and 2.56 Å), accompanied by illite (d—10.05, 4.48, 3.35, 2.86 and 2.57 Å) and kaolinite (d—7.20, 4.48, 3.85, 3.58 and 2.56 Å) were also registered. The X-ray pattern of the sample after firing (0 K) shows some amorphous phase formation (but in much smaller amounts than with the sodium variety sample) and the disappearance of the majority of peaks (especially of illite, kaolinite and albite), except for reflections of quartz and some microcline, the intensity of which weakened markedly. The relatively smaller amorphous phase hump may be a result of the higher melting temperature of potassium feldspar and the smaller alkali content in comparison with sodium samples (8.01% and 8.97% K_2O + Na_2O, respectively). Pure albite $Na[AlSi_3O_8]$ melts congruently at 1118 ± 3 °C, while potassium feldspar $K[AlSi_3O_8]$ melts incongruently at 1150 ± 20 °C, forming the liquid phase containing leucite and silica [12,13]. The latter is characterized by much higher viscosity than the liquid

phase arising in the course of heat treatment of sodium feldspars [14]. Thus, at high temperatures, the glassy phase forms slower and in smaller quantities.
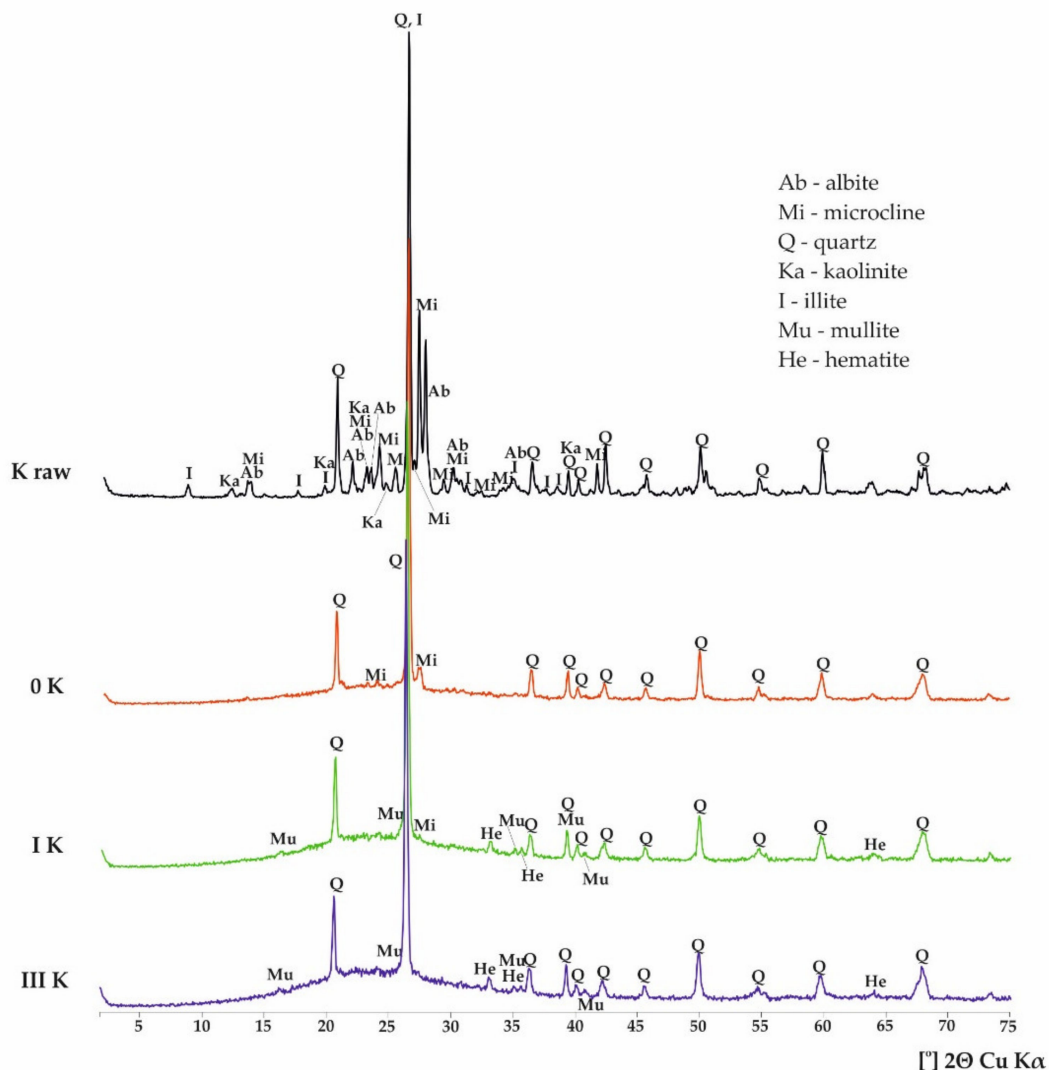
Figure 3. XRD patterns of potassium feldspar-quartz samples in a raw state/unfired (K raw) and the samples after firing: without synthetic pigments addition (0 K), as well as doped with 1.5% Fe_2O_3 (I K), and with 1.5% Fe_2O_3 + 0.5% TiO_2 (III K).

The addition of coloring oxides (I K and III K samples) resulted in the decay of microcline reflections and the appearance of small peaks of mullite (d—5.37, 3.40, 3.39 and 2.29 Å) and of hematite (d—2.69, 2.51, 2.20 and 1.68 Å, albeit of lower intensity than in the X-ray pattern of corresponding sodium samples), as well as raised hump of amorphous phase. The reasons for these differences were similar to the sodium-type material (divalent iron acting as a flux); however, the amount of amorphous phase was notably lower. The peaks of mullite are weaker in the X-ray diffraction pattern of the potassium samples after firing due to the fact that their thermal decomposition takes place at higher temperatures than alkaline feldspars rich in Na_2O. When it comes to sodium feldspars, they turn into the liquid phase faster and secondary mullite crystalizes earlier and more easily. Melting at lower temperature resulted in numerous bubbles that appeared on the surface of the I Na sample (Figure 4), while the surface of the I K pellet was almost free of such irregularities. The peaks of rutile or other titanium phases were not identified. This was probably due to their concentration below the detection limit of the XRD method.

Figure 4. Sodium feldspar-quartz sample doped with 1.5% Fe_2O_3 (I Na) after firing, whose surface is covered with numerous bubbles.
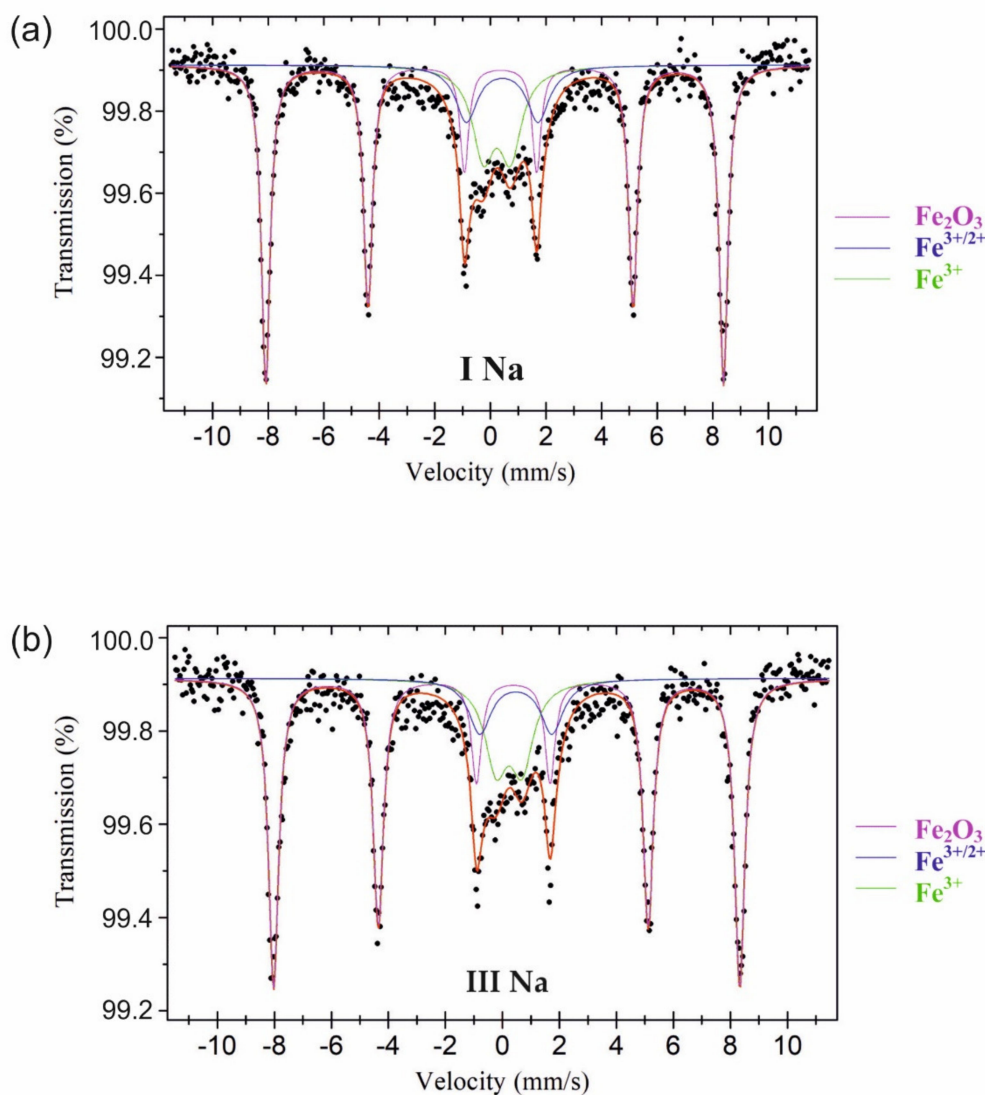
3.3. Mössbauer Spectroscopy

The Mössbauer spectra of both feldspar-quartz varieties doped with synthetic pigments were fitted with three components: one sextet of Fe_2O_3 and two doublets of Fe^{3+} and of $Fe^{3+/2+}$, respectively. The sextet of well crystalized hematite with characteristic hyperfine parameters, i.e., isomer shift IS (0.37 mm/s), quadrupole splitting QS (−0.21 and −0.23 mm/s) and magnetic field B (around 51 T), accounts for around 2/3 (60–68%) of the spectra area (Table 3, Figures 5 and 6). Undeniably, this should be linked to the added synthetic hematite, and possibly to iron ions released from the lattice of other minerals at elevated temperatures that form fine iron oxide particles dispersed in the aluminosilicate matrix [15–18].

Table 3. The results of Mössbauer spectroscopy studies.

Sample	Phase	A (%)	IS (mm/s)	QS (mm/s)	B (T)	Γ (mm/s)
I Na	Fe_2O_3	65 ± 2	0.37	−0.21	51.1	0.28
	$Fe^{3+/2+}$	14 ± 1	0.54	2.57	–	0.90
	Fe^{3+}	21 ± 1	0.34	0.98	–	0.90
III Na	Fe_2O_3	68 ± 2	0.37	−0.23	50.7	0.33
	$Fe^{3+/2+}$	13 ± 1	0.58	2.53	–	0.90
	Fe^{3+}	19 ± 1	0.34	0.91	–	0.90
I K	Fe_2O_3	66 ± 2	0.37	−0.21	51.1	0.26
	$Fe^{3+/2+}$	13 ± 2	0.63	2.43	–	0.93
	Fe^{3+}	21 ± 2	0.34	0.82	–	0.82
III K	Fe_2O_3	60 ± 2	0.37	−0.23	50.7	0.33
	$Fe^{3+/2+}$	16 ± 2	0.58	2.39	–	0.74
	Fe^{3+}	24 ± 2	0.33	0.81	–	0.90

A—relative contribution of the given iron site (sub-spectrum), IS—isomer (total) shift versus α-Fe, QS—quadrupole splitting, B—magnetic hyperfine field, Γ—absorber line-width.

The isomer shift of doublets of Fe^{3+} ions, i.e., IS = 0.33–0.34 (Table 3), is typical for iron oxide compounds [17,18]. However, according to some references, the iron phases present in the raw material can decompose in the course of firing and then iron can be partly or completely diluted in the liquid aluminosilicate phase (at the atomic level) with no separated iron oxide phase [15,18,19] or may be incorporated into the lattice of mullite, substituting for Al^{3+} [20].
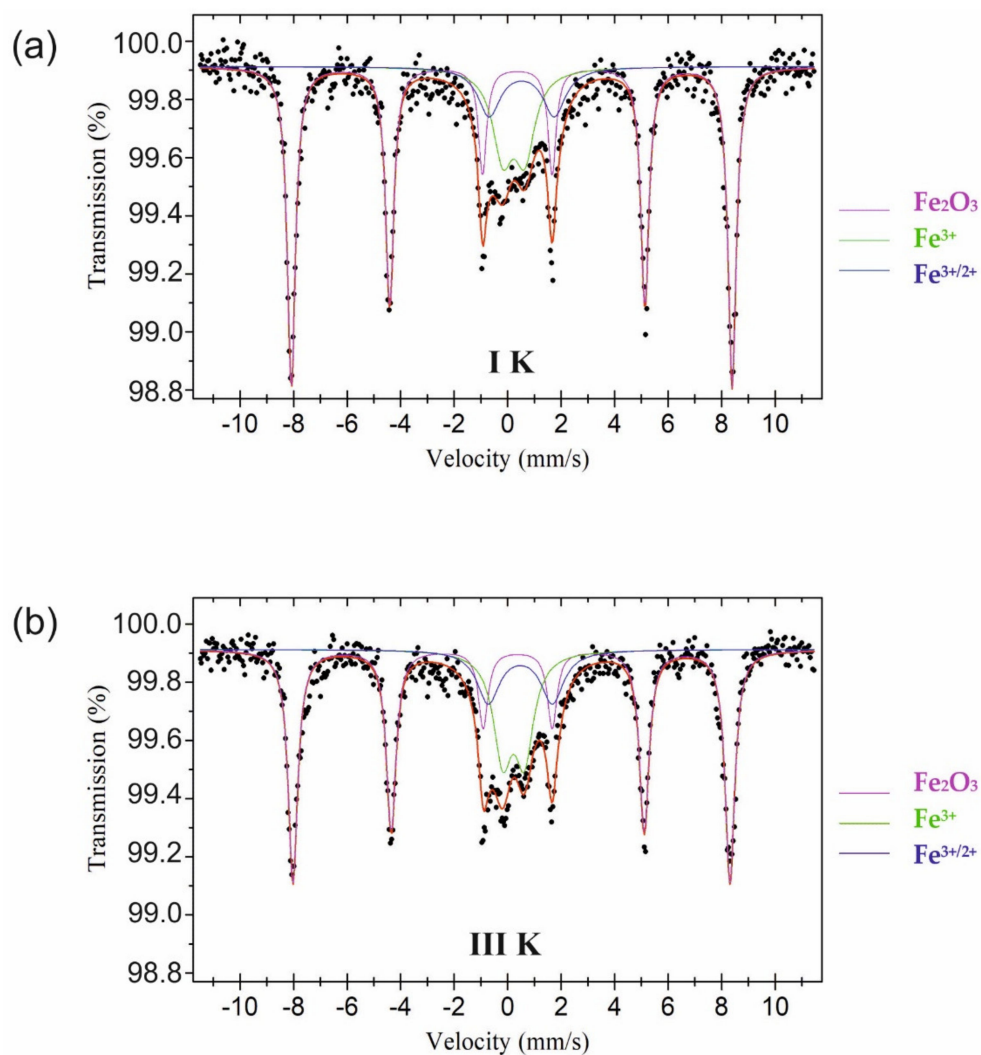
Figure 5. Room temperature Mössbauer spectra of the sodium-rich samples heat-treated at 1200 °C. (**a**) I Na doped with Fe_2O_3, (**b**) III Na doped with $Fe_2O_3 + TiO_2$.

Other components of the analyzed Mössbauer spectra, i.e., doublets of $Fe^{3+/2+}$ are characterized by a quadrupole splitting of about 2.39–2.57 mm/s typical for Fe^{2+} (around 2.5 mm/s) and by an isomer shift of about 0.54–0.63 mm/s assigned to Fe^{3+} in octahedral site (CN = 6). The values of IS are generally in accordance with data in the literature, i.e., 0.35–0.55 mm/s [21] or 0.28–0.50 mm/s [17]. Their relative content ranged from 13% to 16% (Table 3). The presence of $Fe^{3+/2+}$ may be a result of the reduction of some Fe^{3+} ions to Fe^{2+} due to their substitution by Ti^{4+}, following the charge compensation rule [22], as well as of the equilibrium of the Fe^{3+}/Fe^{2+} with the atmospheric partial pressure of oxygen (pO$_2$) [23]. The quadrupole splitting value, which gives the information about local symmetry disorders in the crystal lattice, is much higher for $Fe^{3+/2+}$ (2.39–2.57 mm/s) than that for Fe^{3+} (0.81–0.98 mm/s). This can be linked to possible interactions between Ti and Fe cations (the higher QS, the lower symmetry of the electric charge distribution). Another possible explanation of $Fe^{3+/2+}$ presence is in line with the observations of Bingham et al. [24], according to which the clusters of Fe^{2+}–Fe^{3+} cations can occur in the melts rich in Fe_2O_3. Clustering may include Fe^{2+}–O–Fe^{3+} and Fe^{3+}–O–Fe^{3+} interactions.

The contributions (percentages) of the ^{57}Fe Mössbauer spectral components described above were designated as the area contributions of the corresponding sub-spectra to the whole cross-section of the spectrum. It should be kept in mind that area contributions of the Mössbauer signals discussed here do not necessarily reflect the actual concentrations of the different iron states. Different bond properties of

the iron atoms in their lattice positions lead to different Mössbauer-Lamb factors (MLF), which give rise to different intensities of the Mössbauer signals. In this study, the area contributions of the Mössbauer spectral components are shown and discussed without correction for the possible different values of the MLF, but in fact the MLF for considered materials should have quite similar values and the effects of differential MLF could lead to errors of about 15% for the Fe^{3+}/Fe^{2+} ratio [25,26].

Figure 6. Room temperature Mössbauer spectra of the potassium-rich samples heat-treated at 1200 °C. (**a**) I K doped with Fe_2O_3, (**b**) III K doped with $Fe_2O_3 + TiO_2$.

The relative shares of various forms of iron in the spectra of I K as compared to III K sample, differ from each other: hematite in I K sample is 66% while in III K it is 60% (Table 3). This appears to be related to the presence of TiO_2 and possibly to the potassium nature of the aluminosilicate melt (it is worth noting that the spectra of I Na and III Na samples are almost identical). However, based on the results of Mössbauer spectroscopy measurements, neither the titanium role nor titanium and iron interaction in the case of samples marked III of both varieties of raw materials, can be elucidated.

### 3.4. UV-Vis-NIR Absorbance Spectra

Spectral dependence of the total absorbance in the wavelength range from 220 to 2200 nm measured for selected feldspar-quartz samples after firing is presented in Figure 7. The spectral line shapes of both examined raw material varieties (0 Na, 0 K) are typical for these types of feldspar [27,28]. The presence of a small amount of Fe_2O_3 in the raw materials (0.30–0.36%) gives a clear manifestation in their optical

spectra. In the UV region, a distinct absorption band centered at 262 nm (marked #1) can be observed. It may be assigned to ligand-to-metal charge transfer transitions taking place between O^{2-} and Fe^{3+} ions (OMCT) probably in an octahedral FeO_6 cluster [20,29]. The visible region of the absorbance spectra shows a series of small bands that can be ascribed to d-d transitions within Fe^{3+} ions. They appear at: 384 (#2), 413 (#3), 448 (#4), 487 (#5), 545 (#6), and 642 nm (#7). These bands may be attributable to Fe^{3+} ions in tetrahedral (#2–#4) and octahedral (#5, #6) coordination [30,31]. Some authors [20] ascribe the absorption band at around 448 nm (#4) to d-d transitions of octahedrally coordinated Fe^{3+}. It is worth noting that the aforementioned bands are present in both the potassium and sodium feldspar variety spectrum; however, they are more pronounced in the latter one (0 Na). A weak absorption band at around 860 nm (#8) can be assigned to hematite α-Fe_2O_3 [20,29]. Additionally, between 1000 and 2150 nm a broad band (#9) of weak absorption is observed. Such a band in the near IR may be assigned to the presence of Fe^{2+} ions [20]. The bandwidth can be, according to the literature [32–34], reasonably explained. First and foremost, two bands may overlap, one at around 1100 nm indicating the presence of Fe^{2+} ions in an octahedral sites and another at around 2000 nm corresponding to tetrahedrally coordinated Fe^{2+} ions. The reason for overlapping is probably Jahn-Teller distortion of the octahedrally coordinated iron ions. An additional two bands can be distinguished in the absorption spectra of the examined samples, the first centered at 1420 nm (#10) and the second at 1915 nm (#11). They are much more pronounced in the spectrum of K-type feldspar. According to the literature, these bands may originate from the combination of vibration modes of molecular water occurring in alkali feldspars and quartz in the form of microscopic or sub-microscopic fluid inclusions [34,35]. However, to verify this assumption, the additional investigations would be required. Disparity in absorbance spectra of sodium and potassium feldspar may be attributed to the difference in their chemical properties. The chemical surrounding is affected by atomic properties, especially by ionic radius (K^+—1.38 Å, Na^+—1.02 Å) and electro-negativity (Pauling scale: K^+—0.82, Na^+—0.93).

The shape of the absorbance spectra registered for feldspar-quartz samples doped with Fe_2O_3 synthetic pigment (I Na, I K) is generally similar to these of the basic samples (0 Na, 0 K). Some differences, however, are manifested. First of all, strong absorption band #1 in the UV region is broadened and shifted toward longer wavelengths, up to 390 nm in the visible region. An observed feature can be directly correlated with increased content of Fe^{3+} ions [20]. The red-shift of bands may indicate ligand-to-metal charge transfer transitions occurring between O^{2-} and Fe^{3+} ions as well as the successful incorporation of some Fe^{3+} ions into the lattice of other phases, e.g., mullite as isomorphic substitution for Al^{3+} [20]. The latter assignment seems plausible because the presence of crystalline mullite was evidenced by XRD analysis. As a result, the observed strong absorption may, in fact, be a composite of the mentioned phenomena. Moreover, the intense absorption appeared at around 550 nm. This may be attributed to the simultaneous excitation (magnetic interaction) of adjacent Fe^{3+} cations in the hematite lattice [29]. Above 570 nm the absorbance is much higher than that of undoped materials. The band at 860 nm (#8), assigned to α-Fe_2O_3 (hematite), is significantly stronger than that registered for the raw materials (0 Na, 0 K). Furthermore, a slight shift of the absorption bands arising from Fe^{3+} d-d transitions towards longer wavelengths is also observed. It can be noted that the bands of I K and I Na samples are quite similar and, except for obvious differences in absorbance intensity, resemble the spectrum of undoped sodium sample. Changes in the electronic structure due to increased amount of iron (Pauling electro-negativity of iron is 1.83) eliminate differences caused by distinct chemical properties of sodium and potassium [27,36].

Simultaneous addition of Fe_2O_3 and TiO_2 (III Na, III K) results in further broadening of the strong absorption range (with intensity exceeding 82%) between 220 and 2200 nm. Even though Fe^{3+} bands are less pronounced, their further red-shift in the visible region may be observed. The absorption band at 860 nm (well-defined in the spectra of I K and I Na samples) is much weaker and hardly detectable. Such an effect in combination with the presence of Fe^{3+}-related bands could result from incorporation of Fe^{3+} ions into the lattice of other phases, including TiO_2 and mullite. It should also be noted that

the broad spectral band in the near IR assigned to Fe^{2+} ions is more distinct than that observed in other spectra.
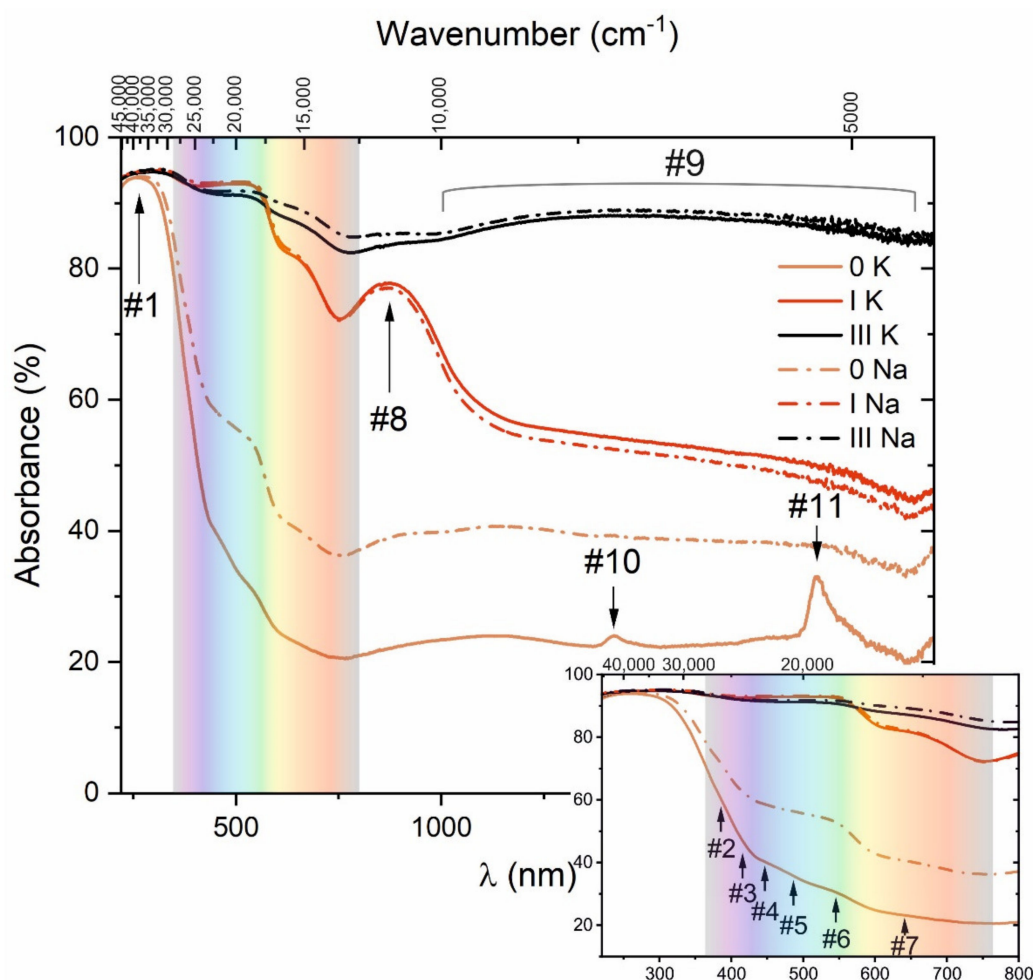
Figure 7. Optical absorbance spectra of selected samples after firing: undoped (0 K, 0 Na), doped with Fe_2O_3 (I K, I Na), and doped with both Fe_2O_3 and TiO_2 (III K, III Na).

3.5. Chromaticity Analysis

To quantify the color of the studied samples and to examine its variation with the iron and titanium content, the CIE (1976) colorimetric system was used (Table 4 and Figure 8). After firing of the potassium-type raw material, the color is brighter compared to that of the sodium type (which is confirmed by the L* coordinate values of 87.71% and 75.86%, respectively). This results from the difference in light absorption in the visible region between both varieties of the studied material, especially in the range of ca. 400–550 nm (Figure 7). The absorption registered for the sodium sample (0 Na) is more intense than that of its potassium counterpart (0 K). The lower the absorption, the more light is reflected from the surface of the sample and the brighter color is perceived. As a consequence, the observed color of 0 Na sample is pale pink, with the corresponding a* value (6.05) much higher than that of 0 K sample (1.67), which is light grey in color (Figure 1, Table 4).

Table 4. Color parameters of the studied samples of different modulus K_2O:Na_2O after firing.

Sample	Color Parameters of the Samples After Firing					
	L*(%)	a*	b*	C*	h*	ΔE
Potassium-rich variety						
0 K	87.71	1.67	9.25	9.40	79.43	
I K	37.76	16.63	10.01	19.41	31.03	47.13
II K	84.56	2.01	15.04	15.17	82.39	5.66
III K	37.61	5.25	4.92	7.19	43.16	44.96
Sodium-rich variety						
0 Na	75.86	6.05	9.68	11.42	57.99	
I Na	36.59	15.91	9.34	18.45	30.41	46.14
II Na	79.45	2.80	11.78	12.11	76.64	3.88
III Na	35.74	3.71	2.56	4.51	34.63	44.97

L*—brightness; a*—red (a > 0); b*—yellow (b > 0); $C^* = (a^2 + b^2)^{1/2}$—chroma/saturation of color; $h^* = \arctan (b/a)$—hue; $\Delta E = \sqrt{(\Delta L^2 + \Delta a^2 + \Delta b^2)}$—total difference of color in relation to basic sample.
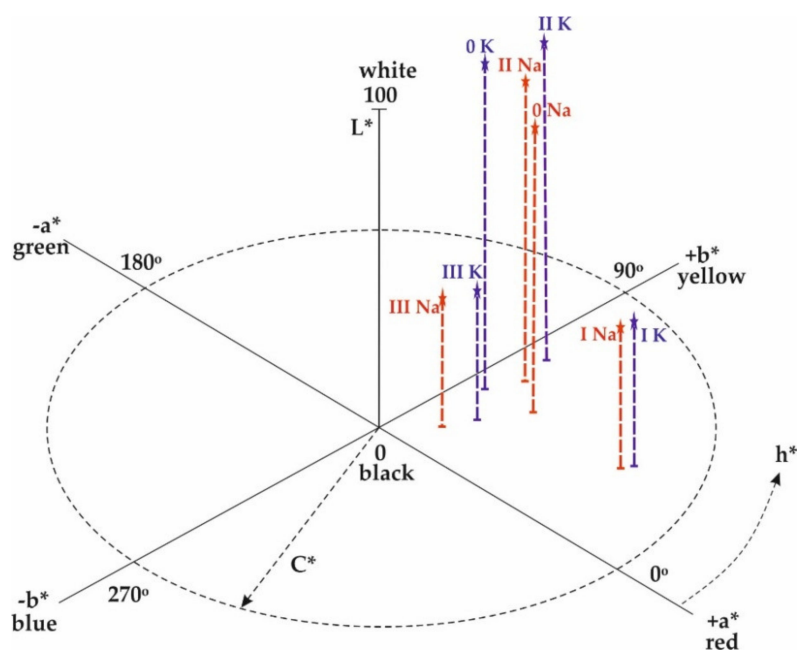
Figure 8. Color parameters of the studied samples in CIE space: K—potassium feldspar-quartz samples, Na—sodium feldspar-quartz samples, 0—basic samples, I—samples doped with 1.5% Fe_2O_3, II—samples doped with 0.5% TiO_2, III—samples doped with 1.5% Fe_2O_3 + 0.5% TiO_2.

Mixing with Fe_2O_3 resulted in decreased brightness L* (to 37.76% and 36.59%, respectively) and hue (h*) of both raw material varieties (Table 4), the change in their coloration was influenced by the hematite added as well as by the breakdown of iron-containing minerals at elevated temperatures with the formation of particles of hematite and Fe^{3+} ions dispersed in the aluminosilicate phase [37–40]. This resulted in strong absorption in the visible region up to 570 nm accompanied by a tint change to dark brown (probably due to d-d electronic transitions in Fe^{3+} ions coupled with Fe^{3+}–Fe^{3+} pair excitation in hematite).

Mixing the studied materials with two synthetic oxides (Fe_2O_3 and TiO_2) caused further significant darkening of their color in relation to samples marked I (doped with Fe_2O_3 only). This was manifested by reduction of brightness L* (to 37.61% and 35.74%, respectively) that resulted from further broadening of the strong absorption range from the visible into the IR part of the spectrum. The addition of TiO_2

caused a distinct change in color of the samples to almost black probably owing to the incorporation of iron ions to the structure of the synthetic rutile and the following charge transfer between Fe and Ti.

4. Discussion

The colors of the fired samples of both raw material varieties doped with two synthetic pigments turned to darker hues than those with the addition of Fe_2O_3 only. This points to an influence of TiO_2. Commercial titanium white is considered to be one of the best white pigments, since pure TiO_2 does not absorb visible light. However, it has been reported that when some iron is present in the structure of TiO_2, a charge transfer between Fe^{2+} and Ti^{4+} ions may occur [41–43]. This can contribute to the optical absorption in the UV and visible range resulting in the change in the coloration of examined samples [31,42–44]. Moreover, there are many colors that are caused by the much weaker electronic transitions between d (or f) orbital energy levels of single transition metal ions, such as Fe [43,45]. These transitions may be strongly intensified by magnetic coupling of adjacent Fe^{3+} cations in the crystal structure of iron phases [29].

Additionally, the presence of iron ions as impurity in raw materials can also contribute to the optical absorption in the UV and visible range due to O–Fe charge transfer (OMCT) [31,42,44]. There is evidence indicating that increasing the iron content causes an increase in the intensity of OMCT bands in the ultraviolet, hence shifting the UV edge towards smaller energies in the visible region [23,24]. This feature was clearly visible especially in the optical spectra of the examined samples doped with synthetic hematite.

On the other hand, the investigations performed by Shi et al. [46] demonstrated that a high content of Fe_2O_3 and TiO_2 in the raw material encourages the formation of a metastable pseudobrookite phase $(Fe^{3+},Fe^{2+})_2(Ti,Fe^{3+})O_5$ coexisting with rutile in the course of the firing. This is in accordance with a ternary phase diagram TiO_2, FeO, Fe_2O_3 [47]. In theory, pseudobrookite should disintegrate during cooling, but in the course of short thermal treatment with relatively low kinetics of this transformation, some remnants of the mentioned phase may remain in the fired material [46,48]. Pseudobrookite can form a solid-state solution with ferropseudobrookite $(Mg^{2+},Fe^{2+},Al^{3+},Fe^{3+})Ti^{4+}_2O_5$ [49,50]. The resulting coexistence of Fe^{2+} and Fe^{3+} in the same structure, may presumably lead to the increase in optical absorption and thus to the change in color. However, these phases have not been detected in the examined samples by XRD analysis, and therefore this hypothesis cannot be confirmed.

Numerous researchers have found that Fe can substitute Ti in the high-temperature melt due to the close ionic radii and valence states of these ions [46,51,52]. According to Kim et al. [53], Ti^{4+} enhances the stability of Fe^{3+} relative to Fe^{2+} in the glassy phase. This is in accordance with the previous work conducted on the redox equilibria of Fe- and Ti-bearing silica glasses, showing the structural instability of the Fe^{2+}–O–Ti^{4+} network [54].

Other reasons for color differences between raw materials of the same or similar coloring oxide contents but of distinct chemical character (sodium or potassium), may be their different behavior during the firing process. The raw material with a higher sodium content forms the liquid phase at lower temperatures than its potassium counterpart. This favors faster phase-to-phase interactions and transition from the crystalline to the liquid state. This may be coupled with releasing iron ions from the lattice of other minerals, which form hematite particles that cause permanent coloring of the material after firing [18]. At high temperatures, some Fe^{3+} ions may be accepted by structures of newly formed mullite at the isomorphic position. Fe^{3+} ions can substitute Al^{3+} ions due to the similar ionic radii of these elements, i.e., Fe^{3+} = 0.55 or 0.59 Å depending on CN, and Al^{3+} = 0.54 Å [18,55].

Furthermore, many investigations have demonstrated a different influence of alkalis, such as K and Na, on iron coordination in various types of silica glasses [23,41–44,56–58]. It has been stated that the presence of larger alkali metal cations (e.g., K^+) facilitates lower metal-oxygen coordination numbers for different transition metal ions, such as Fe^{3+} (ionic radius of K^+ is 1.38 Å, while the ionic radius of Na^+ is 1.02 Å). The valence and coordination of the iron ion have a major effect on the Fe–O bond strength (interionic distance). It was found that replacing K_2O by Na_2O in the silica glasses

containing Fe^{3+} ions resulted in the change of average iron coordination from 4 to 5, while the reversed action caused a marked reduction of CN and the accompanying Fe–O distance. Li et al. [59] revealed that alterations in bond strength between the coloring ions (Fe^{3+}) and the surrounding ligands (O^{2-}) can cause various ligand field splitting energies of Fe-3d levels (for iron present as Fe^{3+} with distorted octahedral geometry) and therefore contribute to different light absorption in the visible light spectrum. Color difference between the fired bodies containing various alkalis (with K_2O or Na_2O prevalence) is clearly visible in the absorption spectra of the studied samples, especially 0 Na and 0 K (undoped with synthetic pigments).

5. Conclusions

The investigations presented here showed that the color of the ceramic body after firing may depend not only on the presence and analytical content of coloring elements (such as iron and titanium), but on their valence state and coordination that induce specific optical transitions as well as on the chemical characteristics of the melt itself (e.g., the prevalence of potassium or sodium ions). This was confirmed using spectroscopic methods and chromaticity measurements.

According to Mössbauer and UV-Vis-NIR analyses, iron is present in the studied samples as hematite α-Fe_2O_3, Fe^{3+}, Fe^{2+} and $Fe^{3+/2+}$ ions (detected by Mössbauer method as Fe cations in oxidation states intermediate between Fe^{2+} and Fe^{3+}). Analysis of optical properties of the raw materials reveal absorption bands resulting from ligand-to-metal charge transfer transitions between oxygen (O^{2-}) and iron (Fe^{3+}) (OMCT) which occur in the UV and stretch into the visible region, especially after doping the examined samples with synthetic pigments. In the visible domain the spectra show a series of absorption bands resulted from d-d electronic transitions within Fe^{3+} ions occupying tetrahedral and/or octahedral coordination. The absorption bands in the near IR region confirm the presence of Fe_2O_3 (hematite) as well as octahedrally coordinated Fe^{2+} ions. Doping with Fe_2O_3 pigment resulted in widening of absorption range in the visible region associated with increased content of Fe^{3+} ions as well as in appearance of the strong and well-defined bands assigned to hematite. These optical features indicate that the majority of synthetic pigment remained unaffected in the course of heat treatment. Simultaneous incorporation of Fe_2O_3 and TiO_2 leads to subsequent broadening of the strong absorption range in the visible and near-IR regions. Weak absorption band attributed to α-Fe_2O_3 in combination with confirmed presence of Fe^{3+} ions may suggest successful doping of iron into TiO_2.

The prevalence of larger alkali cations in the melt (K exceeding Na), is likely to cause a reduction of the coordination number of iron, which has a fundamental effect on the Fe–O bond length. This in turn influences the capacity for light absorption in the visible region. In the case of the sodium-rich variety (0 Na), the absorption (resulting from d-d transitions within Fe^{3+} ions) is much stronger than that recorded for its potassium counterpart (0 K). The addition of synthetic hematite caused an increase in the intensity of OMCT bands registered in the ultraviolet (due to O–Fe charge transfer transitions), hence shifting the UV edge towards the visible region. Furthermore, with increasing Fe concentration, more of the iron ions may occur in adjacent sites, and this probably manifested itself as strong absorption in the visible domain, owing to possible transitions resulting from simultaneous excitation of magnetically coupled Fe^{3+} cations in the hematite lattice. Furthermore, a slight shift of the absorption bands arising from Fe^{3+} d-d transitions towards longer wavelengths was observed. As a consequence, the perceived color of both feldspar-quartz varieties changed into dark brown. Doping with both synthetic pigments (Fe_2O_3 and TiO_2) caused intense absorption (absorbance > 82%) in the whole range of visible light resulting in further darkening of the examined materials which color turned almost black. This could result from charge transfer between Fe and Ti, which has an absorption centered in the near-UV region tailing into the visible and the blue end of the spectrum. However, more complex relationships between Fe and other structural components are possible.

It can be concluded that skillful control of the chemical composition of feldspar-quartz raw materials and precise determination of the redox state of iron can help to obtain ceramic bodies of a required color, notwithstanding the content of coloring oxides in the raw material used.

References

1. Majerowicz, A. On the petrology of the granite massif of Strzegom-Sobótka. *Geol. Sudet.* **1972**, *6*, 83–90.
2. Lewicka, E. The studies of granitoids from the Sobótka region in light of theories of the origin of colour in minerals. *Gosp. Sur. Min.—Miner. Res. Manag.* **2016**, *32*, 55–69. [CrossRef]
3. Lewicka, E. Rational use of selected mining by-products in the ceramic industry in Poland. *Gosp. Sur. Min.—Miner. Res. Manag.* **2020**, *36*, 59–76. [CrossRef]
4. Lewicka, E. Barwa po wypaleniu a skład mineralny kopalin skaleniowych z rejonu Sobótki. *Gosp. Sur. Min.—Miner. Res. Manag.* **2013**, *29*, 35–51. [CrossRef]
5. Lewicka, E. Origin of colour after firing of feldspar-quartz raw material from the Sobótka region (Lower Silesia, SW Poland). In Proceedings of the Mineral Engineering Conference MEC2016, Świeradów-Zdrój, Poland, 25–28 September 2016; Volume 8. Article number 01022. [CrossRef]
6. Lewicka, E. Phase transitions of ferruginous minerals in the course of thermal processing of feldspar-quartz raw materials from the Sobótka region (Lower Silesia). *Gosp. Sur. Min.—Miner. Res. Manag.* **2017**, *33*, 93–110. [CrossRef]
7. Górnicki, R.; Błachowski, A.; Ruebenbauer, K. Mössbauer Spectrometer MsAa-3. *Nukleonika* **2007**, *52* (Suppl. 1), S7.
8. Mysen, B.O.; Virgo, D. Redox equilibria, structure, and properties of Fe-bearing aluminosilicate melts: Relationships among temperature, composition, and oxygen fugacity in the system Na_2O-Al_2O_3-SiO_2-Fe-O. *Am. Mineral.* **1989**, *74*, 58–76.
9. Uchino, T.; Nakaguchi, K.; Nagashima, Y.; Kondo, T. Prediction of optical properties of commercial soda-lime-silicate glasses containing iron. *J. Non-Cryst. Solids* **2000**, *261*, 72–78. [CrossRef]
10. Britt, J. All about iron. *Ceram. Mon.* **2011**, *March 2011*, 14–15.
11. Wilke, M. Fe in magma—An overview. *Ann. Geophys.* **2005**, *48*, 609–617.
12. Ehlers, E.G. *The Interpretation of Geological Phase Diagrams*; W.H. Freeman & Co.: San Francisco, CA, USA, 1972; 280p.
13. Levin, E.M.; Robbins, C.R.; McMurdie, H.F. *Phase Diagrams for Ceramists*, 3rd ed.; The American Ceramic Society: Columbus, OH, USA, 1974; p. 526.
14. Stabile, P.; Webb, S.; Knipping, J.K.; Behrens, H.; Paris, E.; Giuli, G. Viscosity of pantelleritic and alkali-silicate melts: Effect of Fe redox state and Na/(Na+K) ratio. *Chem. Geol.* **2016**, *442*, 73–82. [CrossRef]
15. Stevens, J.G.; Khansanov, A.M.; Miller, J.W.; Pollak, H.; Li, Z. *Mössbauer Mineral Handbook*; Mössbauer Effect Data Center: Asheville, NC, USA, 2005; p. 636.
16. Andji, J.Y.Y.; Abba Toure, A.; Kra, G.; Jumas, J.C.; Yvon, J.; Blanchart, P. Iron role on mechanical properties of ceramics with clays from Ivory Coast. *Ceram. Int.* **2009**, *35*, 571–577. [CrossRef]
17. Menil, F. Systematic trends of the 57Fe Mössbauer isomer shifts in (FeOn) and (FeFn) polyhedra. Evidence of a new correlation between the isomer shift and the inductive effect of the competing bond T-X ($\rightarrow$ Fe) (where X is O or F and T any element with a formal positive charge). *J. Non-Cryst. Solids* **1985**, *46*, 763.
18. Hanzlicek, T.; Niznansky, D.; Dedecek, J.; Steinerova, M.; Straka, P.; Triskova, J. Discoloration of fired kaolinitic clays (study of Fe^{3+} coordination by Mössbauer and UV-ViS-NIR spectroscopy). *J. Am. Ceram. Soc.* **2007**, *9*, 2843–2848. [CrossRef]

19. Soro, N.; Aldon, L.; Olivier-Fourcade, J.; Jumas, J.C.; Laval, J.P.; Blanchart, P. Role of iron in mullite formation from kaolins by Mössbauer spectroscopy and Rietveld refinement. *J. Am. Ceram. Soc.* **2003**, *86*, 129–134. [CrossRef]

20. Djemai, A.; Calas, G.; Muller, J.P. Role of structural Fe(III) and iron oxide nanoparticles in mullite coloration. *J. Am. Ceram. Soc.* **2001**, *84*, 1627–1631. [CrossRef]

21. Dyar, M.D. A review of Mössbauer data on inorganic glasses: The effects of composition on iron valence and coordination. *Am. Mineral.* **1985**, *70*, 304–316.

22. Sorescu, M.; Xu, T.; Wise, A.; Diaz-Michelena, M.; McHenry, M.E. Studies on structural, magnetic and thermal properties of xFe$_2$TiO$_4$-(1-x)Fe$_3$O$_4$ ($0 \leq x \leq 1$) pseudo-binary system. *J. Magn. Magn. Mater.* **2012**, *324*, 1453–1462. [CrossRef]

23. Bingham, P.A.; Hannant, O.M.; Reeves-McLaren, N.; Stennett, M.C.; Hand, R.J. Selective behaviour of dilute Fe^{3+} ions in silicate glasses: An Fe K-edge EXAFS and XANES studies. *J. Non-Cryst. Solids* **2014**, *387*, 47–56. [CrossRef]

24. Bingham, P.A.; Parker, J.M.; Searle, T.; Williams, J.M.; Fyles, K. Redox and clustering of iron in silicate glasses. *J. Non-Cryst. Solids* **1999**, *253*, 203–209. [CrossRef]

25. De Grave, E.; Van Alboom, A. Evaluation of ferrous and ferric Mössbauer fractions. *Phys. Chem. Miner.* **1991**, *18*, 337–342. [CrossRef]

26. Eeckhout, S.G.; De Grave, E. Evaluation of ferrous and ferric Mössbauer fractions. Part II. *Phys. Chem. Miner.* **2003**, *30*, 142–146. [CrossRef]

27. Halmurat, D.; Yusufu, T.; Wang, Q.-L.; He, J.; Sidike, A. Rare earth ion Tb^{3+} doped natural sodium feldspar (NaAlSi$_3$O$_8$). Luminescent properties and energy transfer. *Sci. Rep.* **2019**, *9*, 14637. [CrossRef]

28. Jeong, Y.; Yu, J.; Koh, S.-M.; Heo, C.-H.; Lee, J. Spectral characteristics of minerals associated with skarn deposits: A case study of Weondong skarn deposit South Korea. *Geosci. J.* **2016**, *20*, 167–182. [CrossRef]

29. Sherman, D.M.; Waite, T.D. Electronic spectra of Fe^{3+} oxides and oxide hydroxides in the near IR to near UV. *Am. Mineral.* **1985**, *70*, 1262–1269.

30. Chassé, M.; Lelong, G.; Nijnatten, P.; Schoofs, I.; Wolf, J.; Galoisy, L.; Calas, G. Optical Absorption Microspectroscopy (μ-OAS) Based on Schwarzschild-Type Cassegrain Optics. *Appl. Spectr.* **2015**, *69*, 457–463. [CrossRef]

31. Glebov, L.B.; Boulos, E.N. Absorption of iron and water in the Na$_2$O-CaO-MgO-SiO$_2$ glasses. II. Selection of intrinsic, ferric, and ferrous spectra in the visible and UV regions. *J. Non-Cryst. Solids* **1998**, *242*, 49–62. [CrossRef]

32. Bates, T. Ligand field theory and absorption spectra of transition-metal ions in glasses. In *Modern Aspects of the Vitreous State*; Mackenzie, J.D., Ed.; Butterworths: London, UK, 1962; Volume 2, pp. 195–254.

33. Duffy, J.A. *Bonding, Energy Levels, & Bands*; Longman Group: London, UK, 1990.

34. Smith, J.V.; Brown, W.L. *Feldspar Minerals. Crystal Structures, Physical, Chemical, and Microtextural Properties*, 2nd ed.; Springer-Verlag: Berlin Heidelberg, Germany, 1988; Volume 1. [CrossRef]

35. Johnson, E.A.; Rossmann, G.R. The concentration and speciation of hydrogen in feldspars using FTIR and 1H MAS NMR spectroscopy. *Am. Mineral.* **2003**, *88*, 901–911. [CrossRef]

36. Ahemen, I.; Dejene, F.B. Luminescence and energy transfer mechanism in Eu^{3+}/Tb^{3+}-co-doped ZrO$_2$ nanocrystal rods. *J. Nanopart. Res.* **2017**, *19*, 6. [CrossRef]

37. Torrent, J.; Barron, V. Diffuse reflectance spectroscopy of iron oxides. *Encycl. Surf. Colloid Sci.* **2002**, *1*, 1438–1446.

38. Nodari, L.; Marcuz, E.; Maritan, L.; Mazzoli, C.; Russo, U. Hematite nucleation and growth in the firing of carbonate-rich clay for pottery production. *J. Eur. Ceram. Soc.* **2007**, *27*, 4665–4673. [CrossRef]

39. Opuchovic, O.; Kareiva, A. Historical hematite pigment: Synthesis by an aqueous sol-gel method, characterization and application of the colouration of ceramic glazes. *Ceram. Int.* **2015**, *41*, 4504–4513. [CrossRef]

40. De Bonis, A.; Cultrone, G.; Grifa, C.; Langella, A.; Leone, A.P.; Mercurio, M.; Morra, V. Different shades of red: The complexity of mineralogical and physio-chemical factors influencing the colour of ceramics. *Ceram. Int.* **2017**, *43*, 8065–8074. [CrossRef]

41. Chandrasekhar, S.; Ramaswamy, S. Influence of mineral impurities on the properties of kaolin and its thermally treated products. *Appl. Clay Sci.* **2002**, *21*, 133–142. [CrossRef]

42. Chavoutier, M.; Caurant, D.; Majérus, O.; Boulesteix, R.; Loiseau, P.; Jousseaume, C.; Brunet, E.; Lecomte, E. Effect of TiO$_2$ content on the crystallization and the color of (ZrO$_2$,TiO$_2$)-doped Li$_2$O–Al$_2$O$_3$–SiO$_2$ glasses. *J. Non-Cryst. Solids* **2014**, *384*, 15–24. [CrossRef]

43. Burns, R.G. Intervalence transitions in mixed-valence minerals of iron and titanium. *Ann. Rev. Earth Sci.* **1981**, *9*, 345–383. [CrossRef]

44. Bingham, P.A.; Parker, J.M.; Searle, T.; Smith, I. Local structure and medium range ordering of tetrahedrally coordinated Fe^{3+} ions in alkali-alkaline earth-silica glasses. *J. Non-Cryst. Solids* **2007**, *353*, 2479–2494. [CrossRef]

45. Möncke, D.; Papageorgiou, M.; Winterstein-Beckmann, A.; Zacharias, N. Roman glasses coloured by dissolved transition metal ions: Redox-reactions, optical spectroscopy and ligand field theory. *J. Arch. Sci.* **2014**, *46*, 23–36. [CrossRef]

46. Shi, P.; Wang, F.; Wang, Y.; Zhu, J.; Zhang, B.; Fang, Y. Coloring and translucency mechanism of Five dynasty celadon body from Yaozhou kiln. *Ceram. Int.* **2017**, *43*, 11616–11622. [CrossRef]

47. Taylor, W. System FeO-Fe_2O_3-TiO_2. *J. Am. Ceram. Soc.* **1963**, *46*, 276–279. [CrossRef]

48. Dondi, M.; Matteuci, F.; Cruciani, G.; Gasparotto, G.; Tobaldi, D.M. Pseudobrookite ceramic pigments: Crystal structural, optical and technological properties. *Solid State Sci.* **2007**, *9*, 362–369. [CrossRef]

49. Miyake, A.; Hokada, T. First find of ferropseudobrookite in quartz from Napier Complex, East Antarctica. *Eur. J. Mineral.* **2013**, *25*, 33–38. [CrossRef]

50. Guo, W.Q.; Malus, S.; Ryan, D.H.; Altounian, Z. Crystal structure and cation distribution in the $FeTi_2O_5$-Fe_2TiO_5 solid solution series. *J. Phys. Condens. Mater.* **1999**, *11*, 6337–6346. [CrossRef]

51. Lobacheva, O.; Yiu, Y.M.; Chen, N.; Sham, T.K.; Goncharova, I.V. Changes in local surface structure and Sr depletion in Fe-implemented $SrTiO_3$ (001). *Appl. Surf. Sci.* **2016**, *393*, 74–81. [CrossRef]

52. Bilovol, V.; Ferrari, S.; Derewnicka, D.; Saccone, F.D. XANES and XPS study of electronic structure of Ti-enriched Nd-Fe-B ribbons. *Mater. Chem. Phys.* **2014**, *146*, 269–276. [CrossRef]

53. Kim, J.Y.; No, H.; Jeon, A.Y.; Kim, U.; Pee, J.H.; Cho, W.S.; Kim, K.J.; Kim, C.M.; Kim, C.S. Mössbauer spectroscopic and chromaticity analysis on colorative mechanism of celadon glaze. *Ceram. Int.* **2011**, *37*, 3389–3395. [CrossRef]

54. Alberto, H.V.; Gil, J.M.; Ayres DeCampos, N.; Mysen, B.O. Redox equilibria of iron in Ti-bearing calcium silicate quenched glasses. *J. Non-Cryst. Solids* **1992**, *151*, 39–50. [CrossRef]

55. Handke, M. *Krystalochemia Krzemianów (Chemistry of Silicate Crystals)*; UWN-D: Kraków, Poland, 2008.

56. Brown, G.E., Jr.; Farges, F.; Calas, G. X-ray scattering and X-ray spectroscopy studies of silicate melts. In *Structure, Dynamics and Properties of Silicate Melts, Reviews in Mineralogy and Geochemistry*; Stebbins, J.F., McMillan, P.F., Dingwell, D.B., Eds.; Mineralogical Society of America: Washington, D.C., USA, 1995; Volume 32, pp. 317–410.

57. Farges, F.; Lefrère, Y.; Rossan, S.; Berthereau, A.; Calas, G.; Brown, G.E., Jr. The effect of redox state on the local structural environment of iron in silicate glasses: A molecular dynamics, combined XAFS spectroscopy, and bond valence study. *J. Non-Cryst. Solids* **2004**, *344*, 176–188. [CrossRef]

58. Wilke, M.; Farges, F.; Partzsch, G.M.; Schmidt, C.; Behrens, H. Speciation of Fe in silicate glasses and melts by in-situ XANES spectroscopy. *Am. Mineral.* **2007**, *92*, 44–56. [CrossRef]

59. Li, Y.; Zhang, B.; Cheng, H.; Zheng, J. Revealing the coloration mechanism in the earliest Chinese celadon glaze. *J. Eur. Ceram. Soc.* **2019**, *39*, 1675–1682. [CrossRef]